DIFFIR2VR-ZERO: ZERO-SHOT VIDEO RESTORATION WITH DIFFUSION-BASED IMAGE RESTORATION MODELS

Anonymous authors
Paper under double-blind review

ABSTRACT

This paper introduces a method for zero-shot video restoration using pre-trained image restoration diffusion models. Traditional video restoration methods often need retraining for different settings and struggle with limited generalization across various degradation types and datasets. Our approach uses a hierarchical latent warping strategy for keyframes and local frames, combined with token merging that uses a hybrid correspondence mechanism that integrates spatial information, optical flow, and feature-based matching. We show that our method not only achieves top performance in zero-shot video restoration but also significantly surpasses trained models in generalization across diverse datasets and extreme degradations (8× super-resolution and high-standard deviation video denoising). We present evidence through quantitative metrics and visual comparisons on various challenging datasets. Additionally, our technique works with any 2D restoration diffusion model, offering a versatile and powerful tool for video enhancement tasks without extensive retraining.

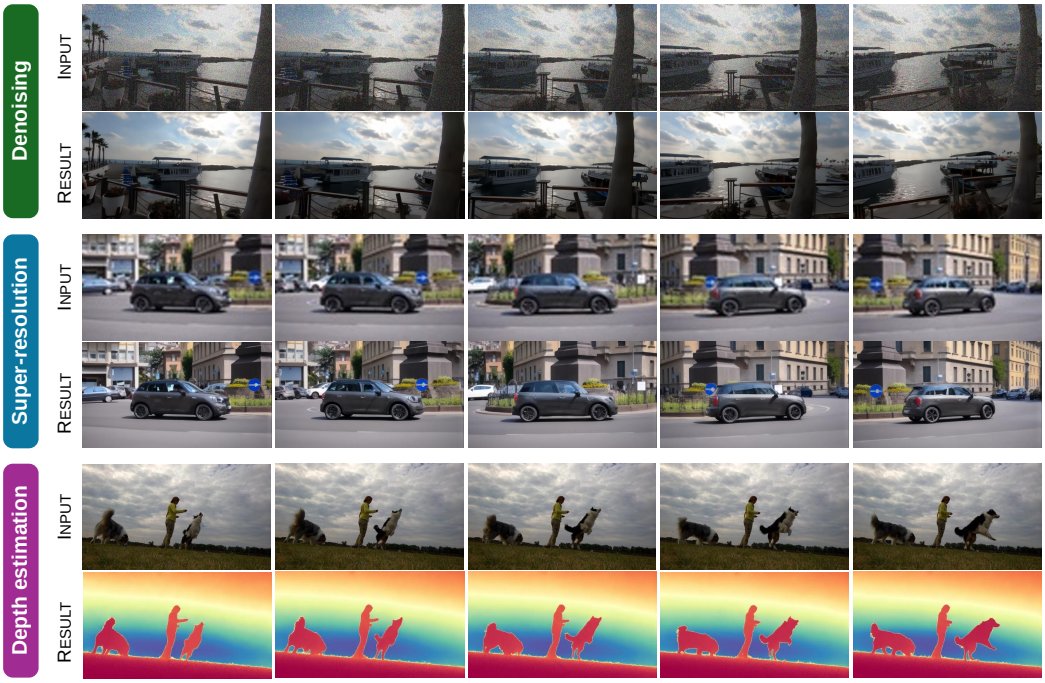

Figure 1: **Zero-shot temporal-consistent diffusion model for video restoration and beyond.** Given a pre-trained diffusion model for *single-image* restoration, our method generates temporally consistent restored video with fine details *without* any further training. Our method applies to other video applications, such as depth estimation.

1 INTRODUCTION

Diffusion models have recently achieved remarkable success in image restoration tasks (Xia et al., 2023; Lin et al., 2024). These models can generate realistic details, overcoming the limitations of traditional regression-based methods that often produce blurry outputs without fine details (Fig. 2 (a)). The state-of-the-art methods employing convolutional neural networks (CNNs) (Albawi et al., 2017; Kalchbrenner et al., 2014; O'shea & Nash, 2015) or transformers (Dosovitskiy et al., 2021; Liu et al., 2021b; Vaswani et al., 2017) trained on large-scale data have shown incredible effectiveness in image restoration.

Given the success of diffusion models in image restoration, a natural extension is to apply them to video restoration. Video restoration, which typically involves denoising, super-resolution, and deblurring, is a valuable field that transforms low-quality videos into high-quality ones. However, directly applying image-based diffusion models to video restoration presents significant challenges. Notably, performing per-frame inference on videos using these models often results in severe flickering (Fig. 2 (b)), especially when using Latent Diffusion Models (LDMs).

Surprisingly, the application of image restoration diffusion models to video restoration remains largely unexplored. While some attempts have been made to adapt these models for video tasks, they typically involve fine-tuning with 3D convolution and temporal attention layers. However, such approaches require extensive computational resources (*e.g.*, 32 A100-80G GPUs for video upscaling (Zhou et al., 2023)) and task-specific retraining, limiting their practicality and generalizability.

In this paper, we present a novel, training-free approach to leverage pre-trained image restoration diffusion models for video restoration. Our method introduces two key modules: hierarchical latent warping and hybrid flow-guided spatial-aware token merging. These modules work in tandem to enforce temporal consistency in both latent and token (feature from the attention layer) spaces, enabling high-quality video restoration without any additional training or fine-tuning. Our method (Fig. 2 (c)) achieves both realistic and temporally consistent results without any additional training, leveraging an image diffusion model to restore videos effectively.

Fig. 1 illustrates our method's capability to generate temporally consistent restored videos across various tasks, including denoising, super-resolution, and depth estimation, *without* any further training. Our zero-shot video restoration framework can be applied to any pre-trained image diffusion model, offering a versatile solution that can adapt to various restoration tasks.

While inspired by recent advances in diffusion-based generation models like VidToMe (Li et al., 2024) and TokenFlow (Geyer et al., 2023), our work goes beyond combining existing techniques. Our main contributions are:

- First zero-shot video restoration using diffusion models, balancing temporal consistency and detail generation across various image-based models.
- Training-free framework manipulating latent and token spaces with hierarchical latent warping and improved token merging.
- State-of-the-art results in extreme scenarios, surpassing traditional methods in generalizability and robustness.

2 RELATED WORK

Video Restoration. Video restoration aims to restore high-quality frames from degraded videos, addressing issues such as noise, blur, and low resolution (Chan et al., 2021a;c; Isobe et al., 2020; Li et al., 2023; Youk et al., 2024; Zhang et al., 2018; Liu et al., 2019; 2021a). This task is more challenging than image restoration due to the need for temporal consistency. Learning-based approaches employ architectures like optical flow warping (Huang et al., 2022; Pan et al., 2020; Shi et al., 2023a;b; Xue et al., 2019), deformable convolutions (Chan et al., 2021a;b; Dai et al., 2017; Tian et al., 2020; Wang et al., 2019; 2020; Zhu et al., 2019), and attention mechanisms to handle temporal dependencies (Cao et al., 2021; Li et al., 2020; Liang et al., 2022; Zamir et al., 2022). Major limitations include dependency on paired HQ-LQ data (Chan et al., 2022; Xie et al., 2023; Yang et al., 2021), assumptions of predefined degradation processes (Kim et al., 2017; 2016; Kong et al., 2023; Li et al., 2020; Liang et al., 2022), and the need for retraining for different degradation levels (Liu & Sun, 2013; Nah et al., 2019; Yi et al., 2019; Youk et al., 2024). These factors reduce effectiveness in real-world applications and lead to poor generalization. Additionally, these methods often lose

Figure 2: **4× video super-resolution results.** (a) Traditional regression-based methods such as FMA-Net (Youk et al., 2024) are limited to the training data domain and tend to produce blurry results when encountering out-of-domain inputs. (b) Although applying image-based diffusion models such as DiffBIR (Lin et al., 2024) to individual frames can generate realistic details, these details often lack consistency across frames. (c) Our method leverages an image diffusion model to restore videos, achieving both realistic and consistent results *without* any additional training.

significant detail, similar to image restoration (Chen et al., 2022; Liang et al., 2021; Wang et al., 2021; Zhang et al., 2021).

Diffusion Models for Image Restoration. With significant advancements in diffusion models (Choi et al., 2021; Dhariwal & Nichol, 2021; Hertz et al., 2023; Ho et al., 2020; Rombach et al., 2022), many diffusion-based approaches have been proposed for image restoration (Fei et al., 2023; Ho et al., 2020; Nichol et al., 2021; Sohl-Dickstein et al., 2015; Song et al., 2020b; Wang et al., 2023; Yang et al., 2023b). These methods include training diffusion models from scratch (Rombach et al., 2022; Saharia et al., 2022; Xia et al., 2023; Yue et al., 2024), introducing constraints into the reverse diffusion process of pre-trained models (Kawar et al., 2022), and fine-tuning frozen pre-trained diffusion models with additional trainable layers (Wang et al., 2023; Yang et al., 2023b; Zhang et al., 2023), as seen in StableSR (Wang et al., 2023) and DiffBIR (Lin et al., 2024). Despite their effectiveness in image restoration, these methods face challenges in video restoration due to temporal inconsistencies caused by the diffusion process's randomness. In contrast, our method allows these approaches to work on video without any training, addressing the temporal consistency issue while leveraging the strengths of image restoration diffusion models.

Video Editing Methods for Temporal Consistency. Recent research has extended pre-trained image diffusion models to video tasks (Esser et al., 2023; Ho et al., 2022a;b; Hu et al., 2023; Lu et al., 2023; Luo et al., 2023; Mei & Patel, 2023; Kara et al., 2024). Various methods have been proposed to enhance temporal consistency in video editing, which can be categorized based on the level at which they operate:

- Latent Space Level: Approaches working at the latent space level include Rerender-A-Video (Yang et al., 2023a), which employs latent warping (Teed & Deng, 2020; Xu et al., 2022) and frame interpolation. While these methods aim to maintain consistency in the latent representations of consecutive frames, they may struggle with semantic consistency in demanding restoration tasks. Our method introduces a novel hierarchical latent warping technique that addresses these limitations.
- Token Level: Methods operating at the token level include VidToMe (Li et al., 2024) and TokenFlow (Geyer et al., 2023), which enhance temporal consistency by merging attention tokens across frames. Token merging (Bolya et al., 2023) is another technique used at this level. However, these techniques often produce blurry outputs in restoration tasks. Our approach improves upon these methods by introducing a hybrid flow-guided spatial-aware token merging technique that maintains sharpness while ensuring temporal consistency.

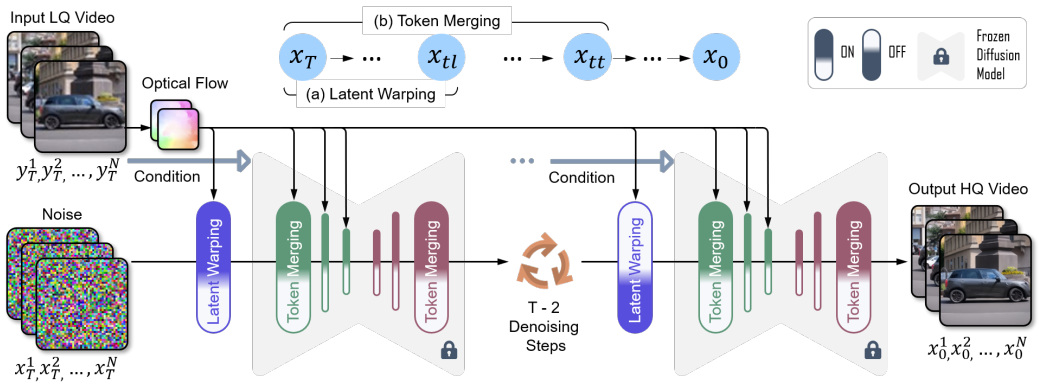

Figure 3: **Pipeline of our proposed zero-shot video restoration method.** We process low-quality (LQ) videos in batches using a diffusion model, with a keyframe randomly sampled within each batch. (a) At the beginning of the diffusion denoising process, hierarchical latent warping provides rough shape guidance both globally, through latent warping between keyframes, and locally, by propagating these latents within the batch. (b) Throughout most of the denoising process, tokens are merged before the self-attention layer. For the downsample blocks, optical flow is used to find the correspondence between tokens, and for the upsample blocks, cosine similarity is utilized. This hybrid flow-guided, spatial-aware token merging accurately identifies correspondences between tokens by leveraging both flow and spatial information, thereby enhancing overall consistency at the token level.

While these video editing techniques generate impressive results with minimal effort, they often struggle with semantic consistency and detail preservation in demanding restoration tasks. Our work draws inspiration from these approaches but introduces novel elements specifically designed to address the challenges of video restoration, combining the strengths of latent and token-level methods while mitigating their individual weaknesses.

3 Method

Given a low-quality video with n frames $\{y^1, y^2, \dots, y^n\}$, we aim to restore it to high-quality $\{x^1, x^2, \dots, x^n\}$ using image-based diffusion models. Directly applying these models frame-by-frame causes temporal inconsistency due to inherent stochasticity, especially in extreme degradation (Fig. 2 and Fig. 6). Our method (Fig. 3) addresses this by enforcing temporal stability in latent and token spaces through Hierarchical Latent Warping (Sec. 3.2) and Hybrid Flow-guided Spatial-aware Token Merging (Sec. 3.3). We introduce diffusion models and video token merging (Sec. 3.1), then detail our key components (Sec. 3.2-Sec. 3.4).

3.1 Diffusion Models for Video Editing

Diffusion models have been successfully applied to video editing tasks by extending image-based models. These models typically operate as follows:

Diffusion Process. The forward process adds noise to a clean image x_0 over T steps:

$$x_t = \sqrt{\alpha_t} x_{t-1} + \sqrt{1-\alpha_t}\epsilon_{t-1} \Rightarrow x_t = \sqrt{\bar{\alpha}_t} x_0 + \sqrt{1-\bar{\alpha}_t}\epsilon, \tag{1}$$

where $t \sim [1, T]$, $\epsilon_t, \epsilon \sim \mathcal{N}(\mathbf{0}, \mathbf{I})$, and $\bar{\alpha}_t = \prod_{s=1}^{t} \alpha_s$. A UNet-based denoiser ϵ_θ is trained to estimate and remove this noise. During inference, the inverse process gradually denoises x_t to produce x_0 (Ho et al., 2020; Song et al., 2020a; 2023). These models can be enhanced with additional guidance signals for controlled generation (Zhang et al., 2023; Kawar et al., 2022).

Video Token Merging. To maintain temporal consistency, techniques like Video Token Merging (VidToMe) (Li et al., 2024) are employed. This process merges similar tokens within frame chunks in attention blocks: Given a token chunk $\mathbf{T} \in \mathbb{R}^{B \times A \times C}$, where $A = w * h$, the algorithm first separates the tokens into source tokens $\mathbf{T}_{\text{src}} \in \mathbb{R}^{B \times A-1 \times C}$ and a target token $\mathbf{T}_{\text{tar}} \in \mathbb{R}^{B \times 1 \times C}$. It then calculates the cosine between each source and target token, determining their corresponding similarity levels, denoted $score \in \mathbb{R}^{((B-1)*A) \times A}$. The algorithm then identifies the most similar target token for each source token by taking the maximum value in the last column.

$$s(\mathbf{T}_{\text{src}}, \mathbf{T}_{\text{tar}}) = \frac{\mathbf{T}_{\text{src}} \cdot \mathbf{T}_{\text{tar}}}{\|\mathbf{T}_{\text{src}}\| \, \|\mathbf{T}_{\text{tar}}\|}, \quad c = \max_{\{\mathbf{t} \in \mathbf{T}_{\text{tar}}\}} (s(\mathbf{T}_{\text{src}}, \mathbf{t})), \tag{2}$$

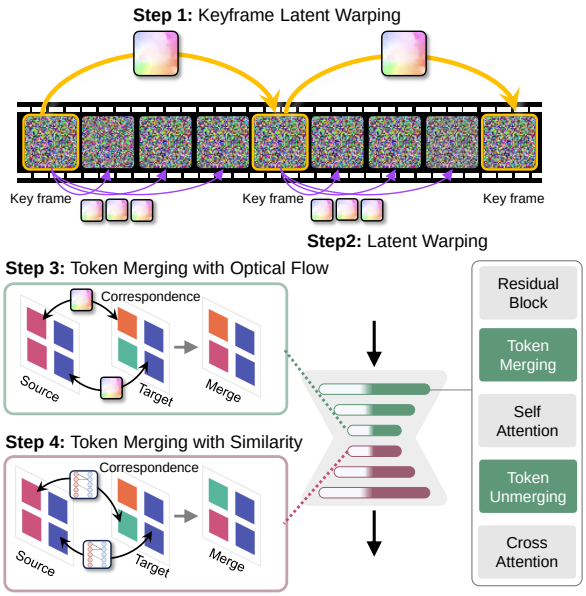

Figure 4: **An illustration of our key modules.** Without requiring any training, these modules can achieve coherence across frames by enforcing temporal stability in both latent and token space. Hierarchical latent warping provides global and local shape guidance; Hybrid spatial-aware token merging before the self-attention layer improves temporal consistency by matching similar tokens using optical flow in the down blocks and cosine similarity in the up blocks of the UNet.

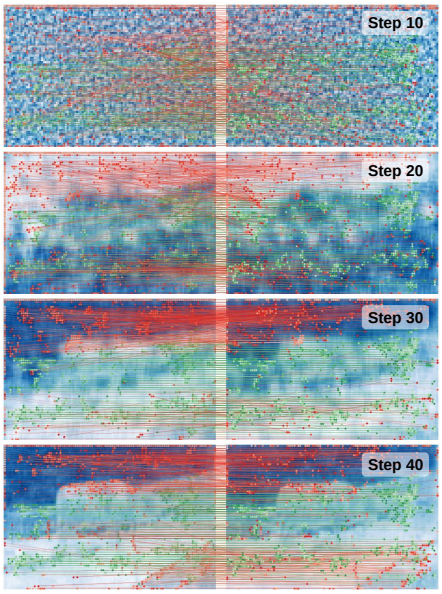

Figure 5: **Token correspondences (cosine similarity and optical flow) across denoising steps.** Early on (e.g. step 10), optical flow guides better due to noisy latents. Later (*e.g.* steps 30-40), similarity and flow focus on different regions, showcasing the benefit of our hybrid approach for effective token merging throughout denoising.

where $s(\cdot,\cdot)$ is the cosine similarity score and c indicates the correspondences. Next, the r most similar paired source-target tokens are merged, and the remaining tokens are concatenated as the output. Merged tokens are subsequently unmerged after self-attention to preserve the original shape by simply assigning the merged source-target tokens the exact same value. The token merging and unmerging are defined as follows:

$$\mathbf{T}_{\text{merge}} = \mathcal{M}(\mathbf{T}_{\text{src}}, \mathbf{T}_{\text{tar}},\ c,\ r)\,,\quad \mathbf{T}_{\text{unmerge}} = \mathcal{U}(\mathbf{T}_{\text{merge}},\ c)\,, \tag{3}$$

where $\mathcal{M}$ and $\mathcal{U}$ denote the merging and unmerging operations, respectively.

Latent Warping. Some methods (Zhou et al., 2023) perform warping in the latent space to maintain consistency between frames. This is done by warping the latent representations of adjacent frames.

Limitations in video restoration. Existing video editing techniques face challenges in video restoration, often prioritizing temporal consistency over detail preservation. Early-stage denoising produces noisy latents, making traditional similarity measures unreliable, especially in UNet's downsample blocks (Fig. 5, top). Most methods focus on frame-to-frame consistency and missing global-local coherence, while high merging ratios can lead to over-smoothing. Our approach combines hierarchical latent warping with hybrid flow-guided spatial-aware token merging to address these limitations. This combination provides multi-scale temporal consistency, balances detail preservation with consistency, and adapts to various degradation types. Latent warping handles large-scale inconsistencies in early stages, while token merging ensures fine detail consistency as features become more meaningful. By leveraging both optical flow and similarity measures, our method aims for superior zero-shot video restoration without task-specific training or computational resources.

3.2 Hierarchical Latent Warping

We introduce a hierarchical latent warping module operating in latent space, with a two-level approach: (1) Global level: Warping between keyframes, and (2) Local level: Propagating warped latents within each batch. As shown in Fig. 4 (upper part), this provides rough shape guidance on global and local

scales. Let $\hat{x}^i_{t\to 0}$ be the predicted $\hat{x}_0$ latent for the ith keyframe at denoising step t. We first perform global-level warping between keyframes:

$$\hat{x}^i_{t\to 0} \leftarrow M_{ji} \cdot \hat{x}^i_{t\to 0} + (1 - M_{ji}) \cdot \mathcal{W}(\hat{x}^j_{t\to 0}, f_{ji}), \tag{4}$$

where $j = i-1$ and f_{ji}, M_{ji} denotes the optical flow and the occlusion mask from lq_j to lq_i estimated by GMFlow (Xu et al., 2022). We then perform local-level warping by propagating these latents to remaining frames within each batch. This approach ensures corresponding points share similar latents globally across keyframes and locally within batches from the start of denoising, providing a more comprehensive approach to maintaining consistency compared to simple frame-to-frame warping.

3.3 Hybrid Flow-guided Spatial-aware Token Merging

While latent manipulation can achieve a certain degree of consistency, manipulating latents during the later stages of the denoising process would result in blurry outcomes. Additionally, the token space is highly semantically related to the image. Therefore, we propose hybrid flow-guided spatial-aware token merging to achieve consistency in the token space.

Flow-guided. Our hybrid correspondence mechanism integrates spatial information, optical flow, and feature-based similarity. In early denoising stages, latents are noisy, making cosine similarity unreliable, especially in UNet's downsample blocks (Fig. 5, top). However, optical flow from low-resolution inputs provides better guidance. As denoising progresses (*e.g.*, steps 30-40), flow-based and similarity-based methods often identify different matches (Fig. 5, bottom), suggesting the benefit of a hybrid approach. Even with low-quality video, we can identify correspondences between frames based on color. We use flow for correspondences in UNet downsample blocks and employ forward-backward consistency check as a criterion to determine r most similar paired source token $\mathbf{T}_{\text{src}}$ and target token $\mathbf{T}_{\text{tar}}$:

$$\sigma = \exp(-\left\| f_{\text{src}\to\text{tar}}(X(\mathbf{T}_{\text{src}})) + f_{\text{tar}\to\text{src}}\left(X(\mathbf{T}_{\text{src}}) + f_{\text{src}\to\text{tar}}(X(\mathbf{T}_{\text{src}}))\right)\right\|_2^2), \tag{5}$$

where σ is the confidence, $X(\mathbf{T}_{\text{src}})$ is the spatial location of $\mathbf{T}_{\text{src}}$, and $f_{src\to tar}$, $f_{tar\to src}$ denotes the forward and backward flow between $\mathbf{T}_{\text{src}}$ and $\mathbf{T}_{\text{tar}}$. The proposed flow-guided token merging is:

$$\mathbf{T}_{\text{merge}} = \mathcal{M}(\mathbf{T}_{\text{src}},\ \mathbf{T}_{\text{tar}},\ f_{\text{src}\to\text{tar}},\ \sigma,\ r). \tag{6}$$

Fig. 4 provides a clearer illustration of our proposed component. While optical flow can be challenging in certain conditions (*e.g.*, fast motion, textureless regions), our method incorporates several safeguards. We use forward-backward consistency checks, merge only the r most similar token pairs, and combine flow-based correspondence with spatial information and similarity matching. This multi-faceted approach ensures robust performance in challenging conditions. Additionally, as shown in Fig. 5 (bottom), flow and cosine similarity identify different correspondences, providing comprehensive guidance. Tab. 1 demonstrates that using flow correspondence in downblocks and similarity in upblocks yields the best visual quality and temporal consistency.

Spatial-awareness and Padding Removal. Directly finding correspondences using cosine similarity can lead to mismatches in areas with uniform textures, especially in video backgrounds (*e.g.*, sky, sand, grass; Fig. 5, bottom), resulting in blurrier outcomes. Given that corresponding points in adjacent frames are typically spatially close, we leverage this information by weighting cosine similarity scores with tokens' spatial distances:

$$s'_{ij} = s_{ij} \cdot e^{-\tau}\ ,\ \text{with}\ \tau = \left\lfloor \left[\|X(i) - X(j)\|_2^2\right] / R \right\rfloor\ , \tag{7}$$

where $X(i)$, $X(j)$ are spatial locations of the ith source and j^{th} target token; R is a hyperparameter defining the radius of the uniform weight region.

This spatial awareness primarily applies to cosine similarity correspondences in UNet upsample blocks. For flow correspondences in downsample blocks, we rely on forward-backward consistency checks as described in Eq. (5), since optical flow models inherently consider spatial information. This combination ensures effective utilization of spatial information throughout our token merging process. Another point to consider is that images are often padded to pass through the UNet, which can significantly impact token correspondences by causing cosine similarity to mistakenly align padding with actual content, even in later denoising stages. To mitigate this, we remove padding before merging and reapply it after unmerging. See the appendix for visual ablation results.

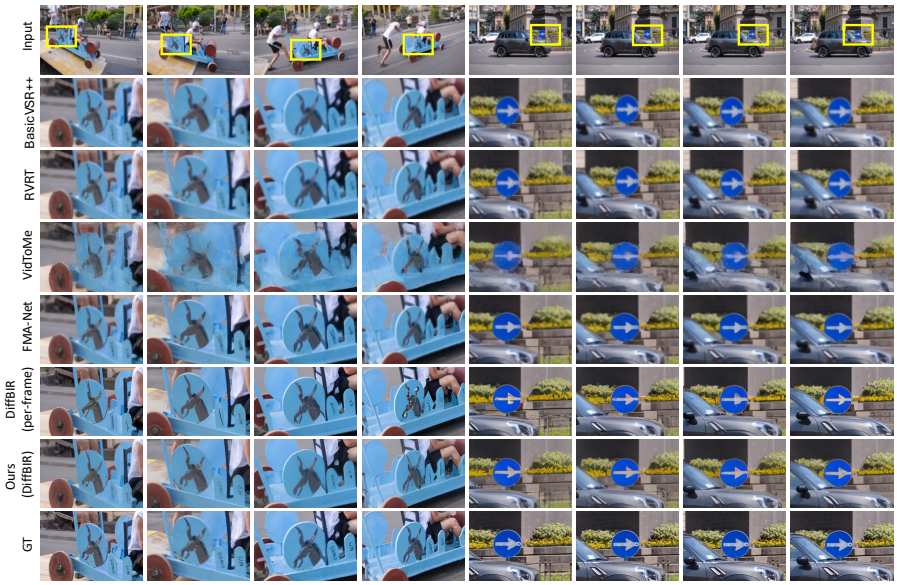

Figure 6: **Qualitative comparisons on 4× video super-resolution.** As shown in the first row, the low-quality input lacks almost all details. In the zoomed-in patches, our method produces clearer and more consistent results.

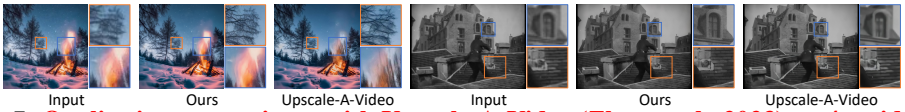

Figure 7: **Qualitative comparisons with Upscale-A-Video (Zhou et al., 2023) on 4× video SR.**

Token Unmerging. After the self-attention operation, tokens need to be unmerged to restore the original shape. We adopt a replacement-based unmerging process where tokens are restored to their original shape using the identified correspondences. This approach is similar to VidToMe (Li et al., 2024), but our method's primary innovation lies in enhancing the correspondence identification process during the merging stage, which leads to more accurate and effective token matching.

Merging Ratio Annealing. To prevent over-smoothing in later denoising stages, we employ ratio annealing to gradually reduce the merging ratio. The merging ratio of the ith denoising step is:

$$r_i = r \cdot \cos\left(\frac{\pi}{2} \cdot \max\left(\min\left(\delta \cdot \frac{i - i_{\text{beg}}}{i_{\text{end}} - i_{\text{beg}}}, 1\right), 0\right)\right), \tag{8}$$

where i_{beg}, i_{end} are predefined steps indicating the beginning and end of the merging process, and δ controls annealing speed. This technique balances smoothness and temporal consistency, achieving a compromise between regression-based methods (temporally consistent but overly smooth) and per-frame inferencing (detailed but inconsistent). As shown in Fig. 2 and Fig. 6, our approach preserves fine details while maintaining temporal coherence, proving effective in severe degradation scenarios. Visual comparisons for 8× super-resolution are provided in supplementary materials.

3.4 Scheduling

As depicted in Fig. 3, at the initial stage of the diffusion denoising process, hierarchical latent warping offers rough shape guidance on a global scale by warping latents between keyframes and on a local scale by propagating these latents within the batch. During the majority of the denoising process, tokens are processed with our hybrid spatial-aware token merging before entering the attention layer. This component further improves temporal consistency by matching similar tokens, utilizing both flow and spatial information.

4 Experiments

Testing Dataset. For video super-resolution, we evaluate on REDS4 (Nah et al., 2019), Vid4 (Liu & Sun, 2013) and DAVIS (Perazzi et al., 2016a) testing sets, with downsample scales ×4 and ×8,

Table 1: **Quantitative comparisons.** (*Left*) Video super-resolution on the DAVIS (Perazzi et al., 2016b), Vid4 (Liu & Sun, 2013) and REDS4 (Nah et al., 2019) datasets. (*Right*) video denoising of various noise levels on the REDS30 and Set8 (Tassano et al., 2019) dataset. The best and second performances are marked in red and blue, respectively. E^*_{warp} denotes $E_{\text{warp}}(\times 10^{-3})$ and E_{inter}, $\text{LPIPS}_{\text{inter}}$ denotes interpolation error and LPIPS. - indicates out-of-memory.

				SD ×4		DiffBIR	
	Metrics	VidToMe	FMA-Net	Frame	Ours	Frame	Ours
DAVIS ×4	PSNR ↑	23.014	25.215	23.504	23.843	23.780	24.182
	SSIM ↑	0.566	0.727	0.584	0.618	0.601	0.621
	LPIPS ↓	0.405	0.347	0.277	0.272	0.264	0.262
	E^*_{warp} ↓	0.520	0.186	0.912	0.745	0.654	0.474
	E_{inter} ↓	13.676	11.558	18.125	17.431	16.529	14.666
	$\text{LPIPS}_{\text{inter}}$ ↓	0.329	0.078	0.292	0.274	0.266	0.232
DAVIS ×8	PSNR ↑	22.097	22.690	20.268	20.519	21.964	22.331
	SSIM ↑	0.513	0.594	0.446	0.424	0.502	0.519
	LPIPS ↓	0.554	0.528	0.470	0.434	0.362	0.367
	E^*_{warp} ↓	0.440	0.351	2.199	1.759	0.964	0.699
	E_{inter} ↓	12.624	13.978	24.496	21.746	17.981	15.853
	$\text{LPIPS}_{\text{inter}}$ ↓	0.388	0.132	0.457	0.442	0.372	0.333
REDS4 ×4	PSNR ↑	23.134	25.829	24.189	24.226	24.679	25.118
	SSIM ↑	0.589	0.761	0.638	0.641	0.657	0.683
	LPIPS ↓	0.357	0.327	0.247	0.242	0.211	0.222
	E^*_{warp} ↓	0.579	0.392	0.817	0.811	0.704	0.499
	E_{inter} ↓	17.869	19.014	22.906	22.889	22.305	20.130
	$\text{LPIPS}_{\text{inter}}$ ↓	0.356	0.133	0.295	0.281	0.271	0.221
REDS4 ×8	PSNR ↑	21.894	22.842	-	-	22.479	22.961
	SSIM ↑	0.532	0.644	-	-	0.559	0.59
	LPIPS ↓	0.538	0.423	-	-	0.311	0.306
	E^*_{warp} ↓	0.423	0.753	-	-	0.828	0.551
	E_{inter} ↓	15.502	21.519	-	-	21.76	19.382
	$\text{LPIPS}_{\text{inter}}$ ↓	0.412	0.159	-	-	0.351	0.287
REDS4 ×16	PSNR ↑	20.520	21.569	18.706	18.858	20.124	20.712
	SSIM ↑	0.483	0.570	0.461	0.410	0.461	0.509
	LPIPS ↓	0.697	0.565	0.612	0.562	0.446	0.438
	E^*_{warp} ↓	0.296	0.619	2.664	2.030	1.168	0.665
	E_{inter} ↓	12.945	18.758	28.478	24.000	21.33	17.731
	$\text{LPIPS}_{\text{inter}}$ ↓	0.417	0.139	0.559	0.493	0.444	0.358
Vid4 ×4	PSNR ↑	19.622	23.209	20.047	20.134	20.687	21.226
	SSIM ↑	0.425	0.679	0.478	0.473	0.497	0.525
	LPIPS ↓	0.491	0.375	0.343	0.331	0.329	0.326
	E^*_{warp} ↓	0.687	0.203	1.502	1.397	1.156	0.677
	E_{inter} ↓	11.754	4.442	17.234	16.921	15.478	11.316
	$\text{LPIPS}_{\text{inter}}$ ↓	0.337	0.026	0.275	0.271	0.265	0.198
Vid4 ×8	PSNR ↑	18.811	21.033	17.813	17.992	18.636	19.304
	SSIM ↑	0.372	0.521	0.345	0.307	0.367	0.406
	LPIPS ↓	0.654	0.514	0.507	0.484	0.440	0.435
	E^*_{warp} ↓	0.477	0.221	2.523	1.972	1.524	0.767
	E_{inter} ↓	9.942	5.269	22.881	19.970	18.112	12.281
	$\text{LPIPS}_{\text{inter}}$ ↓	0.393	0.032	0.423	0.419	0.395	0.294

				DiffBIR	
σ	Metrics	VidToMe	Shift-Net	Frame	Ours
REDS30 75	PSNR ↑	22.671	21.033	24.585	24.520
	SSIM ↑	0.559	0.381	0.649	0.649
	LPIPS ↓	0.397	0.735	0.276	0.275
	E^*_{warp} ↓	0.727	0.765	0.751	0.706
	E_{inter} ↓	18.440	21.751	21.798	21.166
	$\text{LPIPS}_{\text{inter}}$ ↓	0.375	0.501	0.275	0.264
REDS30 100	PSNR ↑	22.588	22.573	24.524	24.534
	SSIM ↑	0.557	0.484	0.648	0.652
	LPIPS ↓	0.404	0.518	0.275	0.271
	E^*_{warp} ↓	0.733	1.126	0.763	0.696
	E_{inter} ↓	18.370	23.424	21.835	20.639
	$\text{LPIPS}_{\text{inter}}$ ↓	0.380	0.375	0.281	0.267
REDS30 random	PSNR ↑	22.348	21.113	24.579	24.508
	SSIM ↑	0.546	0.386	0.650	0.649
	LPIPS ↓	0.429	0.728	0.276	0.270
	E^*_{warp} ↓	0.681	1.896	0.755	0.713
	E_{inter} ↓	17.608	27.565	21.743	21.140
	$\text{LPIPS}_{\text{inter}}$ ↓	0.384	0.542	0.282	0.272
Set8 50	PSNR ↑	21.531	23.433	23.197	23.713
	SSIM ↑	0.501	0.482	0.594	0.63
	LPIPS ↓	0.415	0.574	0.261	0.245
	E^*_{warp} ↓	0.911	1.358	1.078	0.747
	E_{inter} ↓	17.217	19.845	19.732	16.814
	$\text{LPIPS}_{\text{inter}}$ ↓	0.406	0.432	0.332	0.255
Set8 100	PSNR ↑	21.226	18.198	22.519	22.955
	SSIM ↑	0.484	0.281	0.553	0.591
	LPIPS ↓	0.472	0.733	0.338	0.323
	E^*_{warp} ↓	0.918	2.229	1.13	0.802
	E_{inter} ↓	17.367	24.661	20.18	17.444
	$\text{LPIPS}_{\text{inter}}$ ↓	0.421	0.619	0.372	0.286
Set8 150	PSNR ↑	20.209	16.136	21.005	21.418
	SSIM ↑	0.443	0.291	0.486	0.544
	LPIPS ↓	0.554	0.729	0.449	0.402
	E^*_{warp} ↓	0.972	4.279	1.207	0.832
	E_{inter} ↓	17.872	22.343	20.729	17.616
	$\text{LPIPS}_{\text{inter}}$ ↓	0.470	0.646	0.450	0.331

Table 2: **Ablation studies for 8× VSR on DAVIS (Perazzi et al., 2016a) test sets.** (*Left*) different correspondence matching methods. (*Right*) the proposed components applied at different stages of the denoising process. We apply our two proposed components, hierarchical latent warping (HLW) and hybrid spatial-aware token merging (HS-ToMe), at the early, mid, and late denoising stages.

Down blocks	Up blocks	Spatial-aware	LPIPS ↓	E^*_{warp} ↓	$\text{LPIPS}_{\text{inter}}$ ↓
Flow	Flow	–	0.518	1.214	0.563
Cos	Cos	–	0.390	0.736	0.350
Cos	Flow	–	0.507	1.049	0.545
Flow	Cos	–	0.375	**0.677**	0.347
Flow	Cos	✓	**0.367**	0.699	**0.333**

HLW (Sec. 3.2)			HS-ToMe (Sec. 3.3)					
Early	Mid	Late	Early	Mid	Late	LPIPS ↓	E^*_{warp} ↓	$\text{LPIPS}_{\text{inter}}$ ↓
–	–	–	–	–	–	**0.362**	0.964	0.372
✓	–	–	✓	–	–	0.368	0.887	0.369
✓	✓	–	✓	✓	✓	0.43	0.804	0.383
✓	✓	✓	✓	✓	✓	0.411	0.704	0.339
✓	–	–	✓	✓	✓	0.367	**0.699**	**0.333**

following the degradation pipeline of RealBasicVSR (Chan et al., 2022). For video denoising, we evaluate on REDS30 (Nah et al., 2019) and Set8 (Tassano et al., 2020) with different noise levels (std. = 50, 75, 100, 150 and randomly sampled from the range [50, 100]).

Evaluation Metrics. We assess (1) image quality via LPIPS, SSIM, and PSNR; (2) temporal consistency, using warping error E_{warp}, interpolation error, and interpolation LPIPS. Since LPIPS better reflects visual quality, we propose interpolation LPIPS, based on the interpolation error used in a previous study (Li et al., 2024), to more accurately measure video continuity from a visual perspective. This involves interpolating a target frame from its previous and next frames and computing the LPIPS between the estimated and target frames.

Implementation Details. The experiment is conducted on an NVIDIA RTX 4090 GPU. We apply our method to DiffBIR (Lin et al., 2024) and SDx4 upscaler (sdx, 2023), both image-based diffusion

Figure 8: **Video denoising comparisons on the REDS30 (Nah et al., 2019) dataset.** Our method effectively denoises and generates detailed results while maintaining temporal coherence.

models, to demonstrate the proposed method's compatibility with different models. Note that for models that are restricted to a super-resolution scale of 4×, we will apply the process twice and then use bicubic downsampling to achieve 8× results. However, this will can lead to out-of-memory issues for SDx4 upscaler in REDS.

4.1 Comparisons with State-of-the-Art Methods

To verify the effectiveness of our approach, we compare it with several state-of-the-art methods, including FMA-Net (Youk et al., 2024) for video super-resolution, and Shift-Net (Li et al., 2023) for video denoising. We also compare our method to per-frame restoration and the application of VidToMe (Li et al., 2024), a zero-shot video editing method, onto the same model as ours. We also try to compare with Upscale-A-Video (Zhou et al., 2023), which is a diffusion-based video restoration model fine-tuned from an image-based diffusion model. However, due to the lack of released implementation, pre-trained weights, or inference results, we cannot include Upscale-A-Video as a competing method in our comparison.

Our zero-shot video restoration framework is designed to be highly adaptable and capable of leveraging a wide range of pre-trained image diffusion models. This flexibility allows easy adaptation from image to video models without extensive retraining, enabling the application of various restoration tasks by simply switching the underlying image diffusion model.

Video Super-resolution. As shown in Tab. 1, regression-based methods like FMA-Net (Youk et al., 2024) struggle with large motion or severe degradation. VidToMe (Li et al., 2024) can generate highly consistent results, but they are often very blurry, leading to poor visual quality. In contrast, our method enhances temporal consistency while maintaining the generation quality of the original diffusion model, making it the most competitive approach. Fig. 6 provides visualizations of two challenging VSR cases. FMA-Net fails to produce sharp results due to domain gaps between training and testing. Diffusion-based image restoration method DiffBIR (Lin et al., 2024) and SD×4 upscaler (sdx, 2023) can generate sharp results with details, while per-frame processing makes the result video temporal inconsistent and jitters across frames. On the contrary, our zero-shot video restoration framework restores a low-quality input video into a temporally consistent high-quality video.

Video Denoising. Video denoising, compared to VSR, is a simpler task for regression models, as they can often find the correct pixel value given a sufficiently large batch size. However, our method consistently outperforms others in terms of visual quality (LPIPS) and remains highly robust even as degradation becomes severe. Fig. 8 visualizes the denoising results on the REDS30 dataset. Shift-Net (Li et al., 2023) fails to remove all noise, likely due to the out-of-domain noise level; VidToMe (Li et al., 2024) produces smooth results but lacks fine details. Although DiffBIR (Lin et al., 2024) generates highly detailed images, it suffers from poor temporal consistency, as evident in

Figure 9: **Applying our techniques to consistent video depth.** Integrating our proposed framework into Marigold (Ke et al., 2024) helps improve the temporal consistency of video depth estimation.

the changes to the pedestrian's head and the statue's face. In contrast, our method preserves both fine details and temporal consistency, effectively balancing these two aspects.

Other Video Tasks: Consistent Video Depth. Our zero-shot framework is applicable to any pre-trained image-based diffusion models and could improve the predicted video consistency. Therefore, we integrate our proposed zero-shot framework into a state-of-the-art latent diffusion-based monocular depth estimator: Marigold (Ke et al., 2024). Fig. 9 shows that integrating our proposed framework into Marigold helps improve the temporal consistency of video depth estimation. We provide more visual comparisons in the supplementary materials.

This adaptability to various tasks (super-resolution, denoising, depth estimation) showcases the broad applicability of our approach. As more powerful or specialized image models emerge, our framework can quickly adapt to leverage these improvements for video restoration tasks. We provide computational complexity evaluations in the supplementary materials.

4.2 Ablation Study

Ways of Identifying Correspondence. Tab. 2 presents an ablation study comparing different approaches (optical flow and cosine similarity) for finding correspondences and their order in the UNet. As detailed in Sec. 3.3, the hybrid approach of using optical flow at the downsample blocks and cosine similarity at the upsample blocks achieves the best performance. Additionally, our proposed spatial-aware token merging further enhances performance by utilizing spatial information to guide correspondences. See supplementary materials for temporal profile comparisons.

Applied Stages in the Denoising Process. Tab. 2 presents an ablation study evaluating the application of our two proposed components, hierarchical latent warping (HLW, Sec. 3.2) and hybrid spatial-aware token merging (HS-ToMe, Sec. 3.3), at the early, mid, and late stages of the denoising process. The results indicate that applying latent warping in the mid or late stages can significantly degrade the generated outcomes. Furthermore, ensuring consistency in the token space is crucial for achieving coherent and high-quality results.

5 Conclusion

We introduce a novel zero-shot video restoration framework utilizing pre-trained image-based diffusion models, eliminating the need for extensive retraining. Our approach integrates hierarchical latent warping and hybrid flow-guided, spatial-aware token merging, significantly enhancing temporal consistency and video quality under various degradation conditions. Experimental results demonstrate that our framework surpasses existing methods both in quality and consistency.

Limitations. Our framework has two main limitations: (1) LDM decoder sensitivity can cause flickering in dynamic scenes. (2) Extreme degradation may yield unsatisfactory results. Future work will address these issues by stabilizing decoder output, and enhancing extreme degradation handling. Our framework's adaptability allows for the integration of future, more powerful diffusion models.

REFERENCES

Stable diffusion x4 upscaler, 2023. URL https://huggingface.co/stabilityai/stable-diffusion-x4-upscaler.

Saad Albawi, Tareq Abed Mohammed, and Saad Al-Zawi. Understanding of a convolutional neural network. In *2017 international conference on engineering and technology (ICET)*, pp. 1–6. Ieee, 2017.

Daniel Bolya, Cheng-Yang Fu, Xiaoliang Dai, Peizhao Zhang, Christoph Feichtenhofer, and Judy Hoffman. Token merging: Your ViT but faster. In *International Conference on Learning Representations*, 2023.

Jiezhang Cao, Yawei Li, Kai Zhang, and Luc Van Gool. Video super-resolution transformer. *arXiv preprint arXiv:2106.06847*, 2021.

Kelvin CK Chan, Xintao Wang, Ke Yu, Chao Dong, and Chen Change Loy. Basicvsr: The search for essential components in video super-resolution and beyond. In *Proceedings of the IEEE conference on computer vision and pattern recognition*, 2021a.

Kelvin CK Chan, Xintao Wang, Ke Yu, Chao Dong, and Chen Change Loy. Understanding deformable alignment in video super-resolution. In *Proceedings of the AAAI conference on artificial intelligence*, volume 35, pp. 973–981, 2021b.

Kelvin C.K. Chan, Shangchen Zhou, Xiangyu Xu, and Chen Change Loy. Basicvsr++: Improving video super-resolution with enhanced propagation and alignment. 2021c.

Kelvin C.K. Chan, Shangchen Zhou, Xiangyu Xu, and Chen Change Loy. Investigating tradeoffs in real-world video super-resolution. In *IEEE Conference on Computer Vision and Pattern Recognition*, 2022.

Chaofeng Chen, Xinyu Shi, Yipeng Qin, Xiaoming Li, Xiaoguang Han, Tao Yang, and Shihui Guo. Real-world blind super-resolution via feature matching with implicit high-resolution priors. In *Proceedings of the 30th ACM International Conference on Multimedia*, pp. 1329–1338, 2022.

Jooyoung Choi, Sungwon Kim, Yonghyun Jeong, Youngjune Gwon, and Sungroh Yoon. Ilvr: Conditioning method for denoising diffusion probabilistic models. In *Proceedings of the IEEE/CVF International Conference on Computer Vision*, 2021.

Jifeng Dai, Haozhi Qi, Yuwen Xiong, Yi Li, Guodong Zhang, Han Hu, and Yichen Wei. Deformable convolutional networks. In *2017 IEEE International Conference on Computer Vision (ICCV)*, pp. 764–773, 2017. doi: 10.1109/ICCV.2017.89.

Prafulla Dhariwal and Alexander Nichol. Diffusion models beat gans on image synthesis. *Advances in neural information processing systems*, 34:8780–8794, 2021.

Alexey Dosovitskiy, Lucas Beyer, Alexander Kolesnikov, Dirk Weissenborn, Xiaohua Zhai, Thomas Unterthiner, Mostafa Dehghani, Matthias Minderer, Georg Heigold, Sylvain Gelly, Jakob Uszkoreit, and Neil Houlsby. An image is worth 16x16 words: Transformers for image recognition at scale, 2021.

Patrick Esser, Johnathan Chiu, Parmida Atighehchian, Jonathan Granskog, and Anastasis Germanidis. Structure and content-guided video synthesis with diffusion models. In *Proceedings of the IEEE/CVF International Conference on Computer Vision*, pp. 7346–7356, 2023.

Ben Fei, Zhaoyang Lyu, Liang Pan, Junzhe Zhang, Weidong Yang, Tianyue Luo, Bo Zhang, and Bo Dai. Generative diffusion prior for unified image restoration and enhancement. In *Proceedings of the IEEE/CVF Conference on Computer Vision and Pattern Recognition*, pp. 9935–9946, 2023.

Michal Geyer, Omer Bar-Tal, Shai Bagon, and Tali Dekel. Tokenflow: Consistent diffusion features for consistent video editing. *arXiv preprint arXiv:2307.10373*, 2023.

Amir Hertz, Ron Mokady, Jay Tenenbaum, Kfir Aberman, Yael Pritch, and Daniel Cohen-Or. Prompt-to-prompt image editing with cross attention control. In *International Conference on Learning Representations*, 2023.

Jonathan Ho, Ajay Jain, and Pieter Abbeel. Denoising diffusion probabilistic models. *Advances in neural information processing systems*, 33:6840–6851, 2020.

Jonathan Ho, William Chan, Chitwan Saharia, Jay Whang, Ruiqi Gao, Alexey Gritsenko, Diederik P Kingma, Ben Poole, Mohammad Norouzi, David J Fleet, et al. Imagen video: High definition video generation with diffusion models. *arXiv preprint arXiv:2210.02303*, 2022a.

Jonathan Ho, Tim Salimans, Alexey Gritsenko, William Chan, Mohammad Norouzi, and David J Fleet. Video diffusion models. *Advances in Neural Information Processing Systems*, 35:8633–8646, 2022b.

Yaosi Hu, Zhenzhong Chen, and Chong Luo. Lamd: Latent motion diffusion for video generation. *arXiv preprint arXiv:2304.11603*, 2023.

Zhaoyang Huang, Xiaoyu Shi, Chao Zhang, Qiang Wang, Ka Chun Cheung, Hongwei Qin, Jifeng Dai, and Hongsheng Li. Flowformer: A transformer architecture for optical flow. In *European conference on computer vision*, pp. 668–685. Springer, 2022.

Takashi Isobe, Xu Jia, Shuhang Gu, Songjiang Li, Shengjin Wang, and Qi Tian. Video super-resolution with recurrent structure-detail network, 2020.

Nal Kalchbrenner, Edward Grefenstette, and Phil Blunsom. A convolutional neural network for modelling sentences. *arXiv preprint arXiv:1404.2188*, 2014.

Ozgur Kara, Bariscan Kurtkaya, Hidir Yesiltepe, James M. Rehg, and Pinar Yanardag. Rave: Randomized noise shuffling for fast and consistent video editing with diffusion models. In *Proceedings of the IEEE/CVF Conference on Computer Vision and Pattern Recognition*, 2024.

Bahjat Kawar, Michael Elad, Stefano Ermon, and Jiaming Song. Denoising diffusion restoration models. In *Advances in Neural Information Processing Systems*, 2022.

Bingxin Ke, Anton Obukhov, Shengyu Huang, Nando Metzger, Rodrigo Caye Daudt, and Konrad Schindler. Repurposing diffusion-based image generators for monocular depth estimation. In *CVPR*, 2024.

Jiwon Kim, Jung Kwon Lee, and Kyoung Mu Lee. Accurate image super-resolution using very deep convolutional networks. In *Proceedings of the IEEE conference on computer vision and pattern recognition*, pp. 1646–1654, 2016.

Tae Hyun Kim, Seungjun Nah, and Kyoung Mu Lee. Dynamic video deblurring using a locally adaptive blur model. *IEEE transactions on pattern analysis and machine intelligence*, 40(10): 2374–2387, 2017.

Lingshun Kong, Jiangxin Dong, Jianjun Ge, Mingqiang Li, and Jinshan Pan. Efficient frequency domain-based transformers for high-quality image deblurring. In *Proceedings of the IEEE/CVF Conference on Computer Vision and Pattern Recognition*, pp. 5886–5895, 2023.

Dasong Li, Xiaoyu Shi, Yi Zhang, Ka Chun Cheung, Simon See, Xiaogang Wang, Hongwei Qin, and Hongsheng Li. A simple baseline for video restoration with grouped spatial-temporal shift. In *Proceedings of the IEEE/CVF Conference on Computer Vision and Pattern Recognition (CVPR)*, pp. 9822–9832, June 2023.

Wenbo Li, Xin Tao, Taian Guo, Lu Qi, Jiangbo Lu, and Jiaya Jia. Mucan: Multi-correspondence aggregation network for video super-resolution. In *Computer Vision–ECCV 2020: 16th European Conference, Glasgow, UK, August 23–28, 2020, Proceedings, Part X 16*, pp. 335–351. Springer, 2020.

Xirui Li, Chao Ma, Xiaokang Yang, and Ming-Hsuan Yang. Vidtome: Video token merging for zero-shot video editing. In *Proceedings of the IEEE/CVF Conference on Computer Vision and Pattern Recognition*, 2024.

Jingyun Liang, Jiezhang Cao, Guolei Sun, Kai Zhang, Luc Van Gool, and Radu Timofte. Swinir: Image restoration using swin transformer. In *Proceedings of the IEEE/CVF international conference on computer vision*, pp. 1833–1844, 2021.

Jingyun Liang, Yuchen Fan, Xiaoyu Xiang, Rakesh Ranjan, Eddy Ilg, Simon Green, Jiezhang Cao, Kai Zhang, Radu Timofte, and Luc V Gool. Recurrent video restoration transformer with guided deformable attention. *Advances in Neural Information Processing Systems*, 35:378–393, 2022.

Xinqi Lin, Jingwen He, Ziyan Chen, Zhaoyang Lyu, Bo Dai, Fanghua Yu, Wanli Ouyang, Yu Qiao, and Chao Dong. Diffbir: Towards blind image restoration with generative diffusion prior, 2024.

Ce Liu and Deqing Sun. On bayesian adaptive video super resolution. *IEEE transactions on pattern analysis and machine intelligence*, 36(2):346–360, 2013.

Yu-Lun Liu, Yi-Tung Liao, Yen-Yu Lin, and Yung-Yu Chuang. Deep video frame interpolation using cyclic frame generation. In *AAAI*, 2019.

Yu-Lun Liu, Wei-Sheng Lai, Ming-Hsuan Yang, Yung-Yu Chuang, and Jia-Bin Huang. Hybrid neural fusion for full-frame video stabilization. In *ICCV*, 2021a.

Ze Liu, Yutong Lin, Yue Cao, Han Hu, Yixuan Wei, Zheng Zhang, Stephen Lin, and Baining Guo. Swin transformer: Hierarchical vision transformer using shifted windows, 2021b.

Haoyu Lu, Guoxing Yang, Nanyi Fei, Yuqi Huo, Zhiwu Lu, Ping Luo, and Mingyu Ding. Vdt: An empirical study on video diffusion with transformers. *arXiv preprint arXiv:2305.13311*, 2023.

Zhengxiong Luo, Dayou Chen, Yingya Zhang, Yan Huang, Liang Wang, Yujun Shen, Deli Zhao, Jingren Zhou, and Tieniu Tan. Videofusion: Decomposed diffusion models for high-quality video generation. In *Proceedings of the IEEE/CVF Conference on Computer Vision and Pattern Recognition*, pp. 10209–10218, 2023.

Kangfu Mei and Vishal Patel. Vidm: Video implicit diffusion models. In *Proceedings of the AAAI Conference on Artificial Intelligence*, volume 37, pp. 9117–9125, 2023.

Seungjun Nah, Sungyong Baik, Seokil Hong, Gyeongsik Moon, Sanghyun Son, Radu Timofte, and Kyoung Mu Lee. Ntire 2019 challenge on video deblurring and super-resolution: Dataset and study. In *Proceedings of the IEEE/CVF conference on computer vision and pattern recognition workshops*, pp. 0–0, 2019.

Alex Nichol, Prafulla Dhariwal, Aditya Ramesh, Pranav Shyam, Pamela Mishkin, Bob McGrew, Ilya Sutskever, and Mark Chen. Glide: Towards photorealistic image generation and editing with text-guided diffusion models. *arXiv preprint arXiv:2112.10741*, 2021.

Keiron O'shea and Ryan Nash. An introduction to convolutional neural networks. *arXiv preprint arXiv:1511.08458*, 2015.

Jinshan Pan, Haoran Bai, and Jinhui Tang. Cascaded deep video deblurring using temporal sharpness prior. In *Proceedings of the IEEE/CVF conference on computer vision and pattern recognition*, pp. 3043–3051, 2020.

F. Perazzi, J. Pont-Tuset, B. McWilliams, L. Van Gool, M. Gross, and A. Sorkine-Hornung. A benchmark dataset and evaluation methodology for video object segmentation. In *2016 IEEE Conference on Computer Vision and Pattern Recognition (CVPR)*, pp. 724–732, 2016a. doi: 10.1109/CVPR.2016.85.

Federico Perazzi, Jordi Pont-Tuset, Brian McWilliams, Luc Van Gool, Markus Gross, and Alexander Sorkine-Hornung. A benchmark dataset and evaluation methodology for video object segmentation. In *Proceedings of the IEEE conference on computer vision and pattern recognition*, pp. 724–732, 2016b.

Robin Rombach, Andreas Blattmann, Dominik Lorenz, Patrick Esser, and Björn Ommer. High-resolution image synthesis with latent diffusion models. In *Proceedings of the IEEE/CVF conference on computer vision and pattern recognition*, pp. 10684–10695, 2022.

Chitwan Saharia, Jonathan Ho, William Chan, Tim Salimans, David J Fleet, and Mohammad Norouzi. Image super-resolution via iterative refinement. *IEEE transactions on pattern analysis and machine intelligence*, 45(4):4713–4726, 2022.

Xiaoyu Shi, Zhaoyang Huang, Weikang Bian, Dasong Li, Manyuan Zhang, Ka Chun Cheung, Simon See, Hongwei Qin, Jifeng Dai, and Hongsheng Li. Videoflow: Exploiting temporal cues for multi-frame optical flow estimation. In *Proceedings of the IEEE/CVF International Conference on Computer Vision*, pp. 12469–12480, 2023a.

Xiaoyu Shi, Zhaoyang Huang, Dasong Li, Manyuan Zhang, Ka Chun Cheung, Simon See, Hongwei Qin, Jifeng Dai, and Hongsheng Li. Flowformer++: Masked cost volume autoencoding for pretraining optical flow estimation. In *Proceedings of the IEEE/CVF Conference on Computer Vision and Pattern Recognition*, pp. 1599–1610, 2023b.

Jascha Sohl-Dickstein, Eric Weiss, Niru Maheswaranathan, and Surya Ganguli. Deep unsupervised learning using nonequilibrium thermodynamics. In *International conference on machine learning*, pp. 2256–2265. PMLR, 2015.

Jiaming Song, Chenlin Meng, and Stefano Ermon. Denoising diffusion implicit models. *arXiv preprint arXiv:2010.02502*, 2020a.

Yang Song, Jascha Sohl-Dickstein, Diederik P Kingma, Abhishek Kumar, Stefano Ermon, and Ben Poole. Score-based generative modeling through stochastic differential equations. *arXiv preprint arXiv:2011.13456*, 2020b.

Yang Song, Prafulla Dhariwal, Mark Chen, and Ilya Sutskever. Consistency models, 2023.

Matias Tassano, Julie Delon, and Thomas Veit. Dvdnet: A fast network for deep video denoising. In *2019 IEEE International Conference on Image Processing (ICIP)*. IEEE, September 2019. doi: 10.1109/icip.2019.8803136. URL http://dx.doi.org/10.1109/ICIP.2019.8803136.

Matias Tassano, Julie Delon, and Thomas Veit. Fastdvdnet: Towards real-time deep video denoising without flow estimation. In *2020 IEEE/CVF Conference on Computer Vision and Pattern Recognition (CVPR)*, pp. 1351–1360, 2020. doi: 10.1109/CVPR42600.2020.00143.

Zachary Teed and Jia Deng. Raft: Recurrent all-pairs field transforms for optical flow. In *Computer Vision–ECCV 2020: 16th European Conference, Glasgow, UK, August 23–28, 2020, Proceedings, Part II 16*, pp. 402–419. Springer, 2020.

Yapeng Tian, Yulun Zhang, Yun Fu, and Chenliang Xu. Tdan: Temporally-deformable alignment network for video super-resolution. In *Proceedings of the IEEE/CVF conference on computer vision and pattern recognition*, pp. 3360–3369, 2020.

Ashish Vaswani, Noam Shazeer, Niki Parmar, Jakob Uszkoreit, Llion Jones, Aidan N Gomez, Łukasz Kaiser, and Illia Polosukhin. Attention is all you need. *Advances in neural information processing systems*, 30, 2017.

Jianyi Wang, Zongsheng Yue, Shangchen Zhou, Kelvin CK Chan, and Chen Change Loy. Exploiting diffusion prior for real-world image super-resolution. *arXiv preprint arXiv:2305.07015*, 2023.

Xintao Wang, Kelvin CK Chan, Ke Yu, Chao Dong, and Chen Change Loy. Edvr: Video restoration with enhanced deformable convolutional networks. In *Proceedings of the IEEE/CVF conference on computer vision and pattern recognition workshops*, pp. 0–0, 2019.

Xintao Wang, Ke Yu, Kelvin C.K. Chan, Chao Dong, and Chen Change Loy. Basicsr. https://github.com/xinntao/BasicSR, 2020.

Xintao Wang, Liangbin Xie, Chao Dong, and Ying Shan. Real-esrgan: Training real-world blind super-resolution with pure synthetic data. In *Proceedings of the IEEE/CVF international conference on computer vision*, pp. 1905–1914, 2021.

Bin Xia, Yulun Zhang, Shiyin Wang, Yitong Wang, Xinglong Wu, Yapeng Tian, Wenming Yang, and Luc Van Gool. Diffir: Efficient diffusion model for image restoration. In *Proceedings of the IEEE/CVF International Conference on Computer Vision*, pp. 13095–13105, 2023.

Liangbin Xie, Xintao Wang, Shuwei Shi, Jinjin Gu, Chao Dong, and Ying Shan. Mitigating artifacts in real-world video super-resolution models. In *Proceedings of the AAAI Conference on Artificial Intelligence*, volume 37, pp. 2956–2964, 2023.

Haofei Xu, Jing Zhang, Jianfei Cai, Hamid Rezatofighi, and Dacheng Tao. Gmflow: Learning optical flow via global matching. In *Proceedings of the IEEE/CVF Conference on Computer Vision and Pattern Recognition*, pp. 8121–8130, 2022.

Tianfan Xue, Baian Chen, Jiajun Wu, Donglai Wei, and William T Freeman. Video enhancement with task-oriented flow. *International Journal of Computer Vision (IJCV)*, 127(8):1106–1125, 2019.

Zhaoyi Yan, Xiaoming Li, Mu Li, Wangmeng Zuo, and Shiguang Shan. Shift-net: Image inpainting via deep feature rearrangement. In *ECCV*, 2018.

Shuai Yang, Yifan Zhou, Ziwei Liu, and Chen Change Loy. Rerender a video: Zero-shot text-guided video-to-video translation. In *SIGGRAPH Asia 2023 Conference Papers*, pp. 1–11, 2023a.

Tao Yang, Peiran Ren, Xuansong Xie, and Lei Zhang. Pixel-aware stable diffusion for realistic image super-resolution and personalized stylization. *arXiv preprint arXiv:2308.14469*, 2023b.

Xi Yang, Wangmeng Xiang, Hui Zeng, and Lei Zhang. Real-world video super-resolution: A benchmark dataset and a decomposition based learning scheme. In *Proceedings of the IEEE/CVF International Conference on Computer Vision*, pp. 4781–4790, 2021.

Peng Yi, Zhongyuan Wang, Kui Jiang, Junjun Jiang, and Jiayi Ma. Progressive fusion video super-resolution network via exploiting non-local spatio-temporal correlations. In *Proceedings of the IEEE/CVF international conference on computer vision*, pp. 3106–3115, 2019.

Geunhyuk Youk, Jihyong Oh, and Munchurl Kim. Fma-net: Flow-guided dynamic filtering and iterative feature refinement with multi-attention for joint video super-resolution and deblurring. In *CVPR*, 2024.

Zongsheng Yue, Jianyi Wang, and Chen Change Loy. Resshift: Efficient diffusion model for image super-resolution by residual shifting. *Advances in Neural Information Processing Systems*, 36, 2024.

Syed Waqas Zamir, Aditya Arora, Salman Khan, Munawar Hayat, Fahad Shahbaz Khan, and Ming-Hsuan Yang. Restormer: Efficient transformer for high-resolution image restoration. In *Proceedings of the IEEE/CVF conference on computer vision and pattern recognition*, pp. 5728–5739, 2022.

Kai Zhang, Jingyun Liang, Luc Van Gool, and Radu Timofte. Designing a practical degradation model for deep blind image super-resolution. In *Proceedings of the IEEE/CVF International Conference on Computer Vision*, pp. 4791–4800, 2021.

Lvmin Zhang, Anyi Rao, and Maneesh Agrawala. Adding conditional control to text-to-image diffusion models. In *Proceedings of the IEEE/CVF International Conference on Computer Vision*, pp. 3836–3847, 2023.

Yulun Zhang, Yapeng Tian, Yu Kong, Bineng Zhong, and Yun Fu. Residual dense network for image super-resolution. In *Proceedings of the IEEE conference on computer vision and pattern recognition*, pp. 2472–2481, 2018.

Shangchen Zhou, Peiqing Yang, Jianyi Wang, Yihang Luo, and Chen Change Loy. Upscale-a-video: Temporal-consistent diffusion model for real-world video super-resolution. *arXiv preprint arXiv:2312.06640*, 2023.

Xizhou Zhu, Han Hu, Stephen Lin, and Jifeng Dai. Deformable convnets v2: More deformable, better results. In *Proceedings of the IEEE/CVF conference on computer vision and pattern recognition*, pp. 9308–9316, 2019.

A Appendix / supplemental material

In this supplementary material, we first provide additional details on the testing datasets and evaluation metrics. Subsequently, we present more visual comparisons of various methods.

A.1 Ablation studies on correspondences identified by cosine similarity

Fig. 10 The figure shows the correspondences at denoising step 40 for three scenarios: without spatial awareness and padding removal, without spatial awareness, and with both spatial awareness and padding removal (ours). It is evident that padding values significantly affect the matching quality. However, even after removing padding, many mismatched diagonal lines remain, leading to blurry results. In contrast, our method effectively finds accurate correspondences by leveraging spatial information from the video.

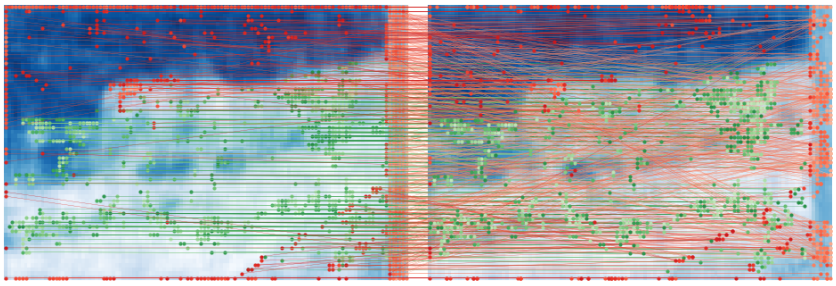

(a) Correspondences without spatial-awareness and padding removal

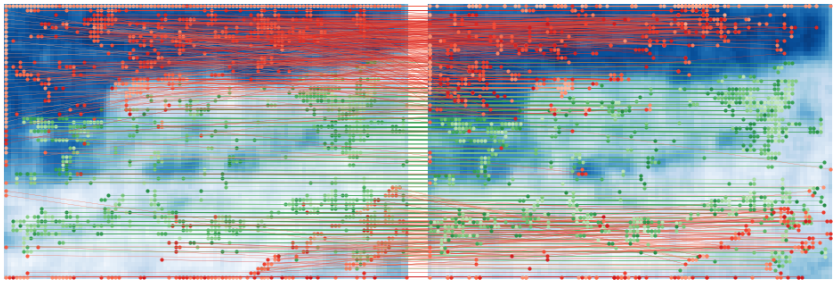

(b) Correspondences without spatial-awareness

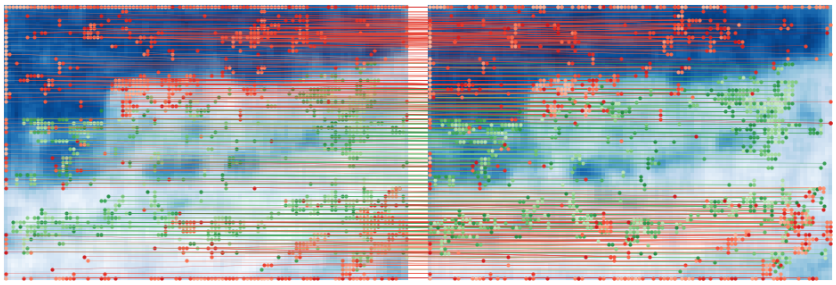

(c) Correspondences with spatial-awareness and padding removal (ours)

Figure 10: **Correspondences at denoising step 40 for different settings.**

A.2 Severe Degradation Scenarios.

Our balanced approach proves particularly effective in severe degradation scenarios. For instance, in 8× super-resolution tasks, our method not only avoids artifacts but can even improve visual quality compared to per-frame approaches (Fig. 11). This underscores the effectiveness of our ratio annealing technique in addressing the over-smoothing tendency while maintaining the benefits of our token merging approach. Additional comparisons on video super-resolution can be found at Fig. 12 and Fig. 13.

Other Video Tasks: Consistent Video Depth. Our zero-shot framework is applicable to any pre-trained image-based diffusion models and could improve the predicted video consistency. Therefore, we integrate our proposed zero-shot framework into a state-of-the-art latent diffusion-based monocular

Figure 11: **Applying our method on DiffBIR and SD ×4 upscaler for 8×SR task.** In this case of severe degradation, our method avoids artifacts and outperforms perframe inference in terms of visual quality.

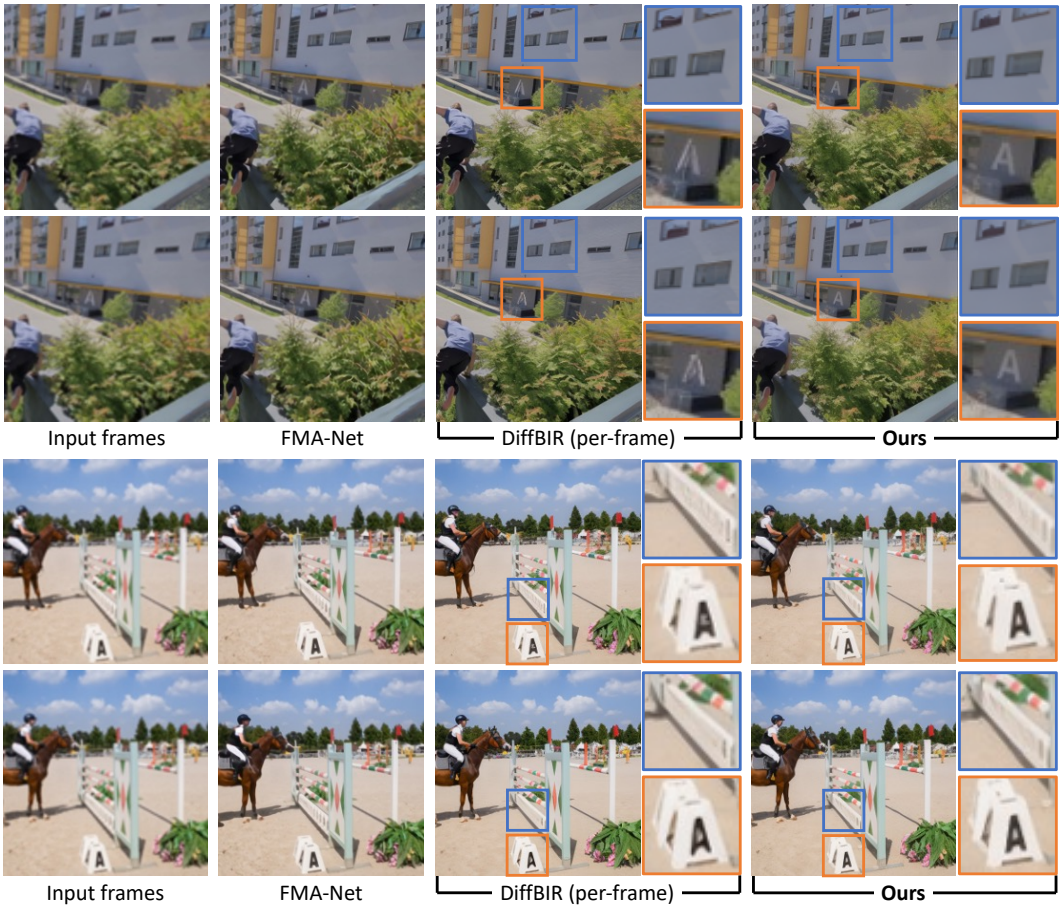

Figure 12: **Additional qualitative comparisons on 4× video super-resolution.** In the zoomed-in patches, our method produces clearer and more consistent results.

depth estimator: Marigold (Ke et al., 2024). Fig. 14 shows that integrating our proposed framework into Marigold helps improve the temporal consistency of video depth estimation.

A.3 Computational Complexity

While our method focuses on zero-shot video restoration without additional training, it's important to consider the computational requirements in comparison to other approaches. Tab. 3 provides an overview of the training time and GPU specifications for different methods, including ours.

As shown in the table, our method stands out by not requiring any training or fine-tuning, which significantly reduces the computational resources needed. This is in stark contrast to other methods

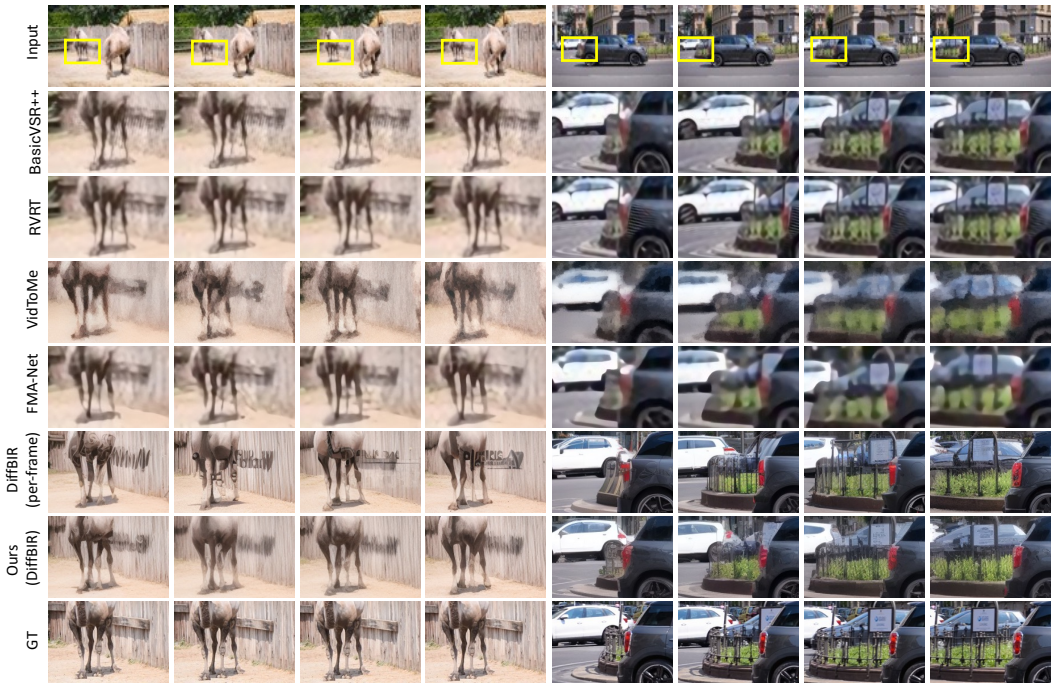

Figure 13: **Additional qualitative comparisons on 8× video super-resolution.** As shown in the first row, the low-quality input lacks almost all details. In the zoomed-in patches, our method produces clearer and more consistent results.

that require multiple high-end GPUs and several days of training time. For inference, our method introduces some computational overhead due to the hierarchical latent warping and hybrid token merging processes. However, this overhead is relatively small compared to the resources required for training or fine-tuning video models. Specifically, our method adds only approximately 6 seconds to the inference time of the base image diffusion model per frame.

Table 3: **Training time and used devices for different methods.**

Method	Training time	GPU specs
Shift-Net (Yan et al., 2018)	Not reported	8 NVIDIA A100-32G GPUs
FMA-Net (Youk et al., 2024)	Not reported	Not reported
Upscale-A-Video (Zhou et al., 2023)	Not reported	32 NVIDIA A100-80G GPUs
Ours	No training needed	-

A.4 Additional Ablation Studies

Comparison of temporal profiles. The comparisons in Fig. 15 also indicate that our results are smoother, demonstrating better temporal stability.

Token Unmerging Strategies. We experimented with two unmerging strategies: averaging paired tokens and direct replacement with keyframe tokens. Tab. 4 shows the results of these experiments on the Vid4 x4 SR task. As shown in the table, the replacement method outperforms averaging in terms of LPIPS, indicating better perceptual quality. Our experiments consistently showed that averaging tends to produce blurrier outputs in restoration tasks. Based on these results, we adopted the replacement-based unmerging process in our final model, as it preserves more details and leads to sharper outputs.

Limitations: Extreme Degradation Extreme degradation (*e.g.*, 32× super-resolution) or overly detailed facial features may yield unsatisfactory results (Fig. 16). However, our framework's adapt-

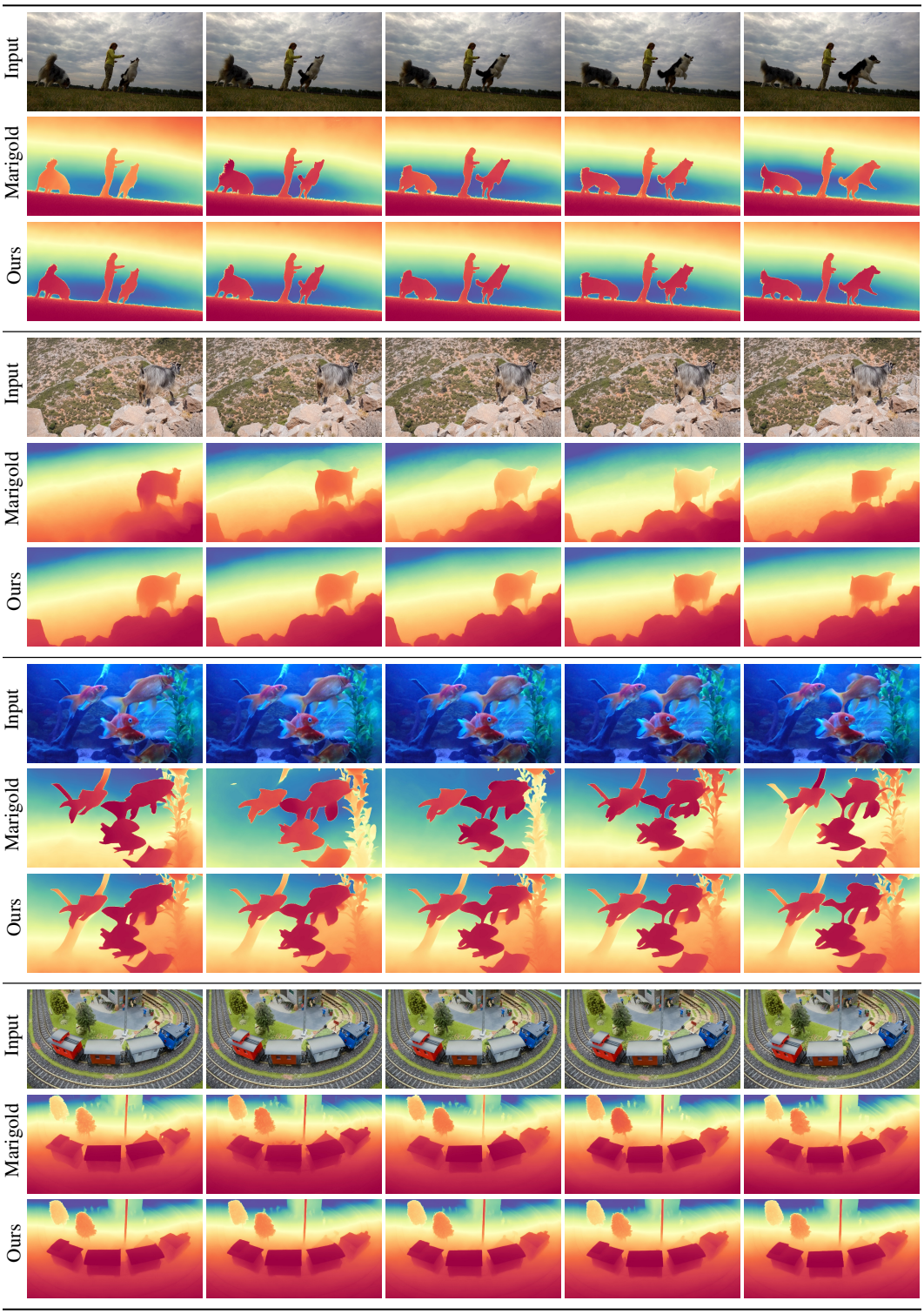

Figure 14: **Applying our techniques to consistent video depth.** Integrating our proposed framework into Marigold (Ke et al., 2024) helps improve the temporal consistency of video depth estimation.

ability allows the incorporation of future, more powerful image-based diffusion models. Future improvements will focus on refining keyframe selection, stabilizing decoder output across LDM ar-

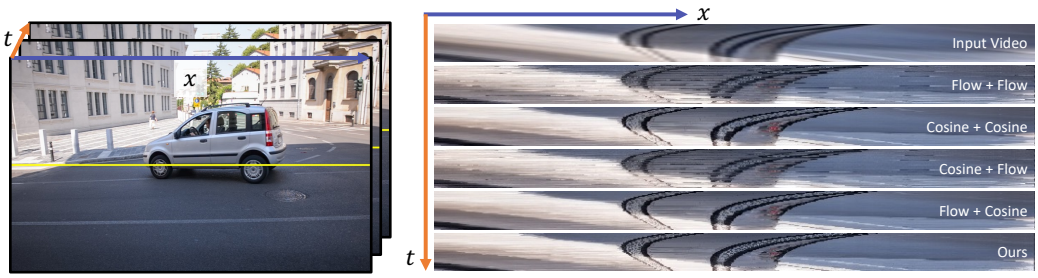

Figure 15: **Comparison of temporal profile.** We examine a row of pixels and track changes over time. The profiles from Flow + Flow and Cosine + Flow methods exhibit noise, indicating flickering artifacts. The Cosine + Cosine method shows smoother profiles but contains some discontinuities. Flow + Cosine demonstrates improved consistency but retains some distortions. Utilizing flow, cosine, and spatial-aware techniques, our method achieves the most seamless and consistent transitions, effectively minimizing artifacts.

Table 4: **Quantitative comparisons of different unmerging methods on Vid4 x4 SR task.**

Unmerging Method	LPIPS ↓
Averaging	0.337
Replacement	0.329

chitectures, and enhancing extreme degradation handling. These aim to improve practical application and mitigate flickering issues inherent in LDM decoders.

(a) DDNM (b) FMA-Net (c) Ours

Figure 16: **Failure case under 32x SR.** Most methods fail under this extreme degradation. However, if more powerful image-based diffusion models emerge in the future, our method can be easily adapted, offering greater potential to achieve this task.